

Boundary layer stagnation-point flow over a stretching/shrinking cylinder in a nanofluid: A stability analysis

Nor Ashikin Abu Bakar^{a,b*}, Norfifah Bachok^b & Norihan Md Arifin^b

^aInstitute of Engineering Mathematics, Universiti Malaysia Perlis, 02600 Arau, Perlis, Malaysia

^bDepartment of Mathematics and Institute for Mathematical Research, Universiti Putra Malaysia, 43400 UPM Serdang, Selangor, Malaysia

Received 16 January 2018; accepted 23 August 2018

The stability analysis of steady boundary layer stagnation-point flow over a stretching/shrinking cylinder using Buongiorno model has been numerically studied. Using similarity transformations the governing partial differential equations have been transformed into a set of nonlinear differential equations and have been solved numerically using a shooting method in Maple software and a *bvp4c* method in Matlab software. These nanofluid model have been used which are taking into account the effects of Brownian motion and thermophoresis. The influences of the governing parameters namely the curvature parameter γ , Prandtl number Pr , Lewis number Le , Brownian motion parameter Nb and thermophoresis parameter Nt on the flow, heat and mass transfers characteristics have been presented graphically. The numerical results obtained for the skin friction coefficient, local Nusselt number and local Sherwood number have been thoroughly determined and presented graphically for several values of the governing parameters. From our investigation, it has been found that the non-unique (dual) solutions exist for shrinking cylinder and a unique solution exist for stretching cylinder. Otherwise, it has been observed that as curvature parameter increases, the skin friction coefficient, heat and mass transfer rates increase. Moreover, the stability analysis shows that the first solution is linearly stable, while the second solution is linearly unstable.

Keywords: Stagnation-point flow, Stretching/shrinking cylinder, Nanofluid, Dual solutions, Stability analysis

1 Introduction

In fluid dynamics, one of the most significant current discussions in the literature is the study of boundary layer stagnation-point flow. Stagnation-point is defined as a point in a flow field where the local velocity of the fluid is zero (rest). The stagnation-point flow over a stretching/shrinking sheet has been investigated by many researchers. This is due to its applications in engineering area such as cooling, nuclear reactor, electronic and many hydrodynamics processes. The preliminary work on the two-dimensional stagnation-point flow over a plate was undertaken by Hiemenz¹. Then, this work was then extended by Homann² where he examined the axisymmetric stagnation-point flow. It is worth mentioning that Crane³ was the first to consider the steady boundary layer flow past a stretching sheet. Next, Chiam⁴ investigated the stagnation-point flow over a stretching sheet. The magnetohydrodynamic stagnation-point flow towards a stretching sheet is discussed by Mahapatra and Gupta⁵. In another study,

Mahaparta and Gupta⁶ also reported the heat transfer in stagnation-point flow towards a stretching sheet. The several physical effects of the stagnation-point flow towards a stretching sheet were discussed by Ishak *et al.*⁷, Layek *et al.*⁸ and Bachok *et al.*⁹. Furthermore, the investigation of the flow past a shrinking was first carried out by Miklavčič and Wang¹⁰. Wang¹¹ then proceed to study the stagnation-point flow past a shrinking sheet. He concluded that the non-unique solutions (dual) exist in the some range of suction. After that, the stagnation-point flow due to shrinking sheet in a micropolar fluid was studied by Ishak *et al.*¹². Lok *et al.*¹³ investigated the MHD stagnation-point flow towards a shrinking sheet. Other studies that related to the stagnation-point flow over a shrinking sheet are Bhattacharyya and Layek¹⁴, Bhattacharyya and Pop¹⁵ and Bhattacharyya *et al.*¹⁶.

The flow over cylinders is considered to be two-dimensional if the body radius is large compared to the boundary layer thickness. Besides, the radius of the thin or slender cylinder may be of the same order as that of the boundary layer thickness. Therefore, the

*Corresponding author (E-mail: ashikinbakar@unimap.edu.my)

flow may be considered as axisymmetric instead of two-dimensional as studied by Datta *et al.*¹⁷ and Kumari and Nath¹⁸. There are some applications on the flow over a stretching or shrinking cylinder in industrial and engineering processes. Simal *et al.*¹⁹ developed a sample shrinkage model, which is useful for the simulation of the drying curves of broccoli stems at different air drying temperatures and sample lengths, thus can predict the 1668 drying times and end-point of a drying process. They also insisted that their model could be applied to simulate the drying curves of different biological and cylindrical products. The study of steady flow in a viscous fluid over a stretching cylinder has been investigated by Wang²⁰. Ishak *et al.*²¹ examined the effects of uniform suction/blowing on the flow and heat transfer due to a stretching cylinder. Again, Ishak *et al.*²² discussed the MHD flow and heat transfer analysis over a stretching cylinder. Wang and Ng²³ investigated the slip flow due to a stretching cylinder. Meanwhile, Wang²⁴ proposed the study of natural convection on a vertical stretching cylinder. Next, the unsteady viscous flow over a shrinking cylinder with mass transfer is analyzed by Wan Zaimi *et al.*²⁵. The steady stagnation-point flow of a viscous and incompressible fluid over a permeable shrinking circular cylinder was discovered by Lok and Pop²⁶. Then, Mat *et al.*²⁷ presented the study of the stagnation-point slip flow and heat transfer towards a shrinking/stretching cylinder over a permeable surface.

Nanofluid is a fluid that contains nanometer-sized particles, which called nanoparticles. The term “nanofluid” was first proposed by Choi²⁸. The nanofluid are potential to increase thermal conductivity and consequently, enhances the heat transfer characteristics. Abel *et al.*²⁹ mentioned that nanofluids potentially used in microelectronics, fuel cells, pharmaceutical processes, hybrid-power engine, engine cooling, domestic refrigerator and chiller. Buongiorno³⁰ was the first who introduced the model for convective transport in nanofluids with the effects of Brownian diffusion and thermophoresis. Yet, very few studies examined the flow over stretching/shrinking cylinder using this nanofluid model. Rasekh *et al.*³¹ have analyzed the flow and heat transfer over a stretching cylinder in a nanofluid. Moreover, Noghrehabadi *et al.*³² researched the MHD flow on the boundary layer, heat and mass transfer of nanofluids over a stretching cylinder. Later, Tiwari and Das³³ introduced the nanofluid model that

considers the effect of nanoparticle volume fraction. Gorla *et al.*³⁴ studied the melting heat transfer in a nanofluid boundary layer on a stretching circular cylinder. Then, Omar *et al.*³⁵ examined the stagnation point flow over a stretching/shrinking cylinder in a copper-water nanofluid. Recently, Sulochana and Sandeep³⁶ investigated the stagnation point flow and heat transfer behaviour of copper-water nanofluid towards horizontal stretching/shrinking cylinder.

This present study is an extension of the work reported earlier by Bachok *et al.*³⁷ to the case of stretching/shrinking cylinder, which using the Buongiorno³⁰ nanofluid model. The study explores the effect of the Brownian motion and thermophoresis as well as curvature parameter on the flow, heat and mass transfer rates behaviours. Besides, the stability solution solutions have been carried out since we expect that the dual solutions can be obtained. The work on stability analysis can be found in the paper of Merkin³⁸, Weidman *et al.*³⁹, Harris *et al.*⁴⁰, Najib *et al.*⁴¹ and Bakar *et al.*⁴² for different cases.

2 Mathematical Formulation

Consider a steady stagnation-point flow towards a stretching/shrinking cylinder with radius R placed in incompressible nanofluid of constant temperature T_w . It is assumed that the free stream velocity is $U_\infty = cx/L$ and the stretching/shrinking velocity is $U_w = ax/L$ where a and c are constant with $c > 0$ corresponds to stretching constant, $c < 0$ corresponds to shrinking constant, x is the coordinate measured along the cylinder and L is the characteristics length. The physical model for stagnation-point flow in cylinder is presented in Fig. 1. The boundary layer equations^{35,37} can be written as:

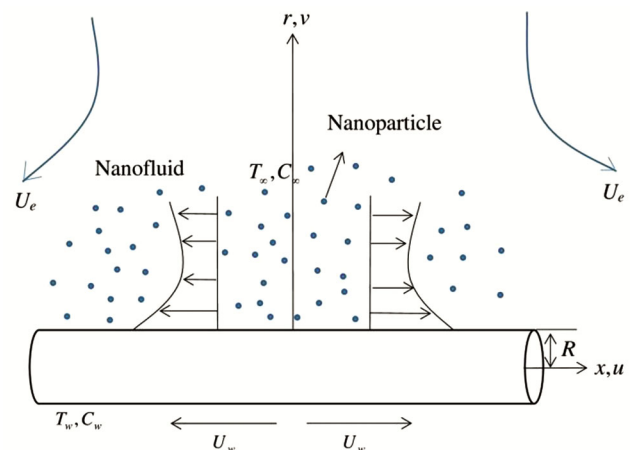


Fig. 1 — Physical model for stagnation-point flow in cylinder.

$$\frac{\partial}{\partial x}(ru) + \frac{\partial}{\partial r}(rv) = 0, \quad \dots (1)$$

$$u \frac{\partial u}{\partial x} + v \frac{\partial u}{\partial r} = U_\infty \frac{dU_\infty}{dx} + v \left(\frac{\partial^2 u}{\partial r^2} + \frac{1}{r} \frac{\partial u}{\partial r} \right), \quad \dots (2)$$

$$u \frac{\partial T}{\partial x} + v \frac{\partial T}{\partial r} = \alpha \left(\frac{\partial^2 T}{\partial r^2} + \frac{1}{r} \frac{\partial T}{\partial r} \right) + \tau \left[D_B \frac{\partial C}{\partial r} \frac{\partial T}{\partial r} + \frac{D_T}{T_\infty} \left(\frac{\partial T}{\partial r} \right)^2 \right], \quad \dots (3)$$

$$u \frac{\partial C}{\partial x} + v \frac{\partial C}{\partial r} = D_B \left(\frac{\partial^2 C}{\partial r^2} + \frac{1}{r} \frac{\partial C}{\partial r} \right) + \frac{D_T}{T_\infty} \left(\frac{\partial^2 T}{\partial r^2} + \frac{1}{r} \frac{\partial T}{\partial r} \right), \quad \dots (4)$$

where x and r are the coordinates measured along the surface of the cylinder and in the radial direction, respectively, with u and v being the corresponding velocity components. Next, T is the temperature in the boundary layer, C is the nanoparticle concentration in the boundary layer, ν is the kinematic viscosity coefficient, D_B is the Brownian diffusion coefficient, D_T is the thermophoresis diffusion coefficient, $\alpha = k/(\rho c)_f$ is the thermal diffusivity of the fluid and $\tau = (\rho c)_p/(\rho c)_f$ is the ratio between the effective heat capacity of the nanoparticle material and heat capacity of the fluid with ρ_f is the density of the fluid, ρ_p is the density of the particles and c is the volumetric volume expansion coefficient. The boundary conditions are:

$$u = U_w(x), \quad v = 0, \quad T = T_w, \quad C = C_w \quad \text{at } r = R, \\ u \rightarrow U_\infty, \quad T \rightarrow T_\infty, \quad C \rightarrow C_\infty \quad \text{as } r \rightarrow \infty. \quad \dots (5)$$

We look for similarity solutions of Eqs (1) to (4), subject to boundary conditions Eq. (5) by introducing the similarity transformations³⁵:

$$\eta = \frac{r^2 - R^2}{2R} \left(\frac{c}{\nu L} \right)^{1/2}, \quad \psi = \left(\frac{\nu c}{L} \right)^{1/2} x R f(\eta), \quad \dots (6) \\ \theta(\eta) = \frac{T - T_\infty}{T_w - T_\infty}, \quad \phi(\eta) = \frac{C - C_\infty}{C_w - C_\infty},$$

where η is the similarity variable and ψ is the stream function defined as $u = r^{-1} \partial \psi / \partial y$ and $v = -r^{-1} \partial \psi / \partial x$ which identically satisfies Eq. (1). By defining η in this form, the boundary conditions at

$r = R$ reduce to the boundary conditions at $\eta = 0$, which is more convenient for the numerical computations.

Substituting Eq. (6) into Eqs (2), (3) and (4), we obtain the following nonlinear ordinary differential equations:

$$(1 + 2\eta\gamma)f''' + 2\gamma f'' + ff'' - f'^2 + 1 = 0, \quad \dots (7)$$

$$\frac{1}{Pr} [(1 + 2\eta\gamma)\theta'' + 2\gamma\theta'] + f\theta' \\ + (1 + 2\eta\gamma)Nb\theta'\phi' + (1 + 2\eta\gamma)Nt\theta'^2 = 0, \quad \dots (8)$$

$$(1 + 2\eta\gamma)\phi'' + Le f\phi' + 2\gamma\phi' \\ + (1 + 2\eta\gamma)\frac{Nt}{Nb}\theta'' + 2\gamma\frac{Nt}{Nb}\theta' = 0, \quad \dots (9)$$

subjected to the boundary conditions (5) which becomes:

$$f(0) = 0, \quad f'(0) = \varepsilon, \quad \theta(0) = 1, \quad \phi(0) = 1, \\ f'(\eta) \rightarrow 1, \quad \theta(\eta) \rightarrow 0, \quad \phi(\eta) \rightarrow 0 \quad \text{as } \eta \rightarrow \infty, \quad \dots (10)$$

where $\varepsilon = a/c$ is stretching/shrinking parameter, with $\varepsilon > 0$ corresponds to stretching sheet and $\varepsilon < 0$ corresponds to shrinking sheet. In the above equations, prime denote differentiation with respect to η and the other parameters are defined by:

$$Pr = \frac{\nu}{\alpha}, \quad Le = \frac{\nu}{D_B}, \quad Nb = \frac{(\rho c)_p D_B (C_w - C_\infty)}{(\rho c)_f \nu}, \\ Nt = \frac{(\rho c)_p D_T (T_w - T_\infty)}{(\rho c)_f T_\infty \nu}, \quad \gamma = \left(\frac{\nu L}{cR^2} \right)^{1/2}. \quad \dots (11)$$

where Pr is the Prandtl number, Le is the Lewis number, Nb is the Brownian motion parameter, Nt is the thermophoresis parameter and γ is the curvature parameter.

The physical quantities of interest are the skin friction coefficient C_f , local Nusselt number Nu_x and local Sherwood number Sh_x defined as:

$$C_f = \frac{\tau_w}{\rho U_\infty^2}, \quad Nu_x = \frac{xq_w}{k(T_w - T_\infty)}, \quad \dots (12)$$

$$Sh_x = \frac{xq_m}{D_B(C_w - C_\infty)},$$

where the wall shear stress τ_w , the local heat flux q_w and the local mass flux q_m as follows:

$$\tau_w = \mu \left(\frac{\partial u}{\partial r} \right)_{r=R}, \quad q_w = -k \left(\frac{\partial T}{\partial r} \right)_{r=R}, \quad \dots (13)$$

$$q_m = -D_B \left(\frac{\partial T}{\partial r} \right)_{r=R},$$

with μ and k are the dynamic viscosity of the nanofluids and the thermal conductivity of the nanofluids, respectively.

Using the similarity variables (6), the reduced skin friction coefficient, local Nusselt number and local Sherwood number are:

$$C_f \text{Re}_x^{1/2} = f''(0), \quad Nu_x \text{Re}_x^{-1/2} = -\theta'(0), \quad \dots (14)$$

$$Sh_x \text{Re}_x^{-1/2} = -\phi'(0),$$

where $\text{Re}_x = U_\infty x / \nu$ is the local Reynolds number.

3 Stability Analysis

The numerical results obtained show that for a certain range of ε , there exist two branches of solutions for different values of γ . In order to determine which of these solutions are stable, a stability analysis is performed. According to Weidman *et al.*³⁹ and Rosca and Pop⁴³, it is shown that the upper branch solutions are stable (physically realizable), while the lower branch solutions are unstable (not physically realizable). We consider the unsteady form of Eqs (2)-(4) and introducing the new dimensionless time variable³⁹ τ . The new variables for the unsteady problem are:

$$\eta = \frac{r^2 - R^2}{2R} \left(\frac{c}{\nu L} \right)^{1/2}, \quad \psi = \left(\frac{\nu c}{L} \right)^{1/2} x R f(\eta, \tau), \quad \dots (15)$$

$$\theta(\eta, \tau) = \frac{T - T_\infty}{T_w - T_\infty}, \quad \phi(\eta, \tau) = \frac{C - C_\infty}{C_w - C_\infty}, \quad \tau = \frac{ct}{L}.$$

The governing Eqs (2)-(4) become

$$(1 + 2\eta\gamma) \frac{\partial^3 f}{\partial \eta^3} + 2\gamma \frac{\partial^2 f}{\partial \eta^2} + f \frac{\partial^2 f}{\partial \eta^2} \quad \dots (16)$$

$$- \left(\frac{\partial f}{\partial \eta} \right)^2 + 1 - \frac{\partial^2 f}{\partial \eta \partial \tau} = 0,$$

$$\frac{1}{\text{Pr}} \left[(1 + 2\eta\gamma) \frac{\partial^2 \theta}{\partial \eta^2} + 2\gamma \frac{\partial \theta}{\partial \eta} \right] + f \frac{\partial \theta}{\partial \eta} \quad \dots (17)$$

$$+ (1 + 2\eta\gamma) Nb \frac{\partial \theta}{\partial \eta} \frac{\partial \phi}{\partial \eta}$$

$$+ (1 + 2\eta\gamma) Nt \left(\frac{\partial \theta}{\partial \eta} \right)^2 - \frac{\partial \theta}{\partial \tau} = 0,$$

$$(1 + 2\eta\gamma) \frac{\partial^2 \phi}{\partial \eta^2} + Le f \frac{\partial \phi}{\partial \eta} + 2\gamma \frac{\partial \phi}{\partial \eta} \quad \dots (18)$$

$$+ (1 + 2\eta\gamma) \frac{Nt}{Nb} \frac{\partial^2 \theta}{\partial \eta^2} + 2\gamma \frac{Nt}{Nb} \frac{\partial \theta}{\partial \eta} - Le \frac{\partial \phi}{\partial \tau} = 0,$$

subject to boundary conditions

$$f(0, \tau) = 0, \quad \frac{\partial f}{\partial \eta}(0, \tau) = \varepsilon, \quad \theta(0, \tau) = 1,$$

$$\phi(0, \tau) = 1,$$

$$\frac{\partial f}{\partial \eta}(\eta, \tau) \rightarrow 1, \quad \theta(\eta, \tau) \rightarrow 0, \quad \dots (19)$$

$$\phi(\eta, \tau) \rightarrow 0 \text{ as } \eta \rightarrow \infty.$$

To test the stability of the steady flow solution $f(\eta) = f_0(\eta)$, $\theta(\eta) = \theta_0(\eta)$ and $\phi(\eta) = \phi_0(\eta)$ satisfying the boundary-value problem (2) - (4), can be written as:

$$f(\eta, \tau) = f_0(\eta) + e^{-\varpi \tau} F(\eta, \tau), \quad \dots (20)$$

$$\theta(\eta, \tau) = \theta_0(\eta) + e^{-\varpi \tau} G(\eta, \tau),$$

$$\phi(\eta, \tau) = \phi_0(\eta) + e^{-\varpi \tau} H(\eta, \tau),$$

where ϖ is an unknown Eigen value, and $F(\eta, \tau)$, $G(\eta, \tau)$ and $H(\eta, \tau)$ are small relative to $f_0(\eta)$, $\theta_0(\eta)$ and $\phi_0(\eta)$, respectively. The solution of the Eigen value problem (16)-(18) give an infinite set of Eigen values $\varpi_1 < \varpi_2 < \dots$; if the smallest Eigen value is negative, there is an initial growth of disturbances and the flow is unstable; but when ϖ_1 is positive, there is an initial decay and the flow is stable. By introducing (20) into (16) - (18), followed by setting $\tau = 0$, and hence substituting $F = F_0(\eta)$, $G = G_0(\eta)$ and $H = H_0(\eta)$, the linearized problem is given by:

$$(1 + 2\eta\gamma) F_0''' + 2\gamma F_0'' + f_0 F_0'' \quad \dots (21)$$

$$+ f_0'' F_0 - 2f_0' F_0' + \varpi F_0' = 0,$$

$$\frac{1}{\text{Pr}} \left[(1 + 2\eta\gamma) G_0'' + 2\gamma G_0' \right] + f_0 G_0' \quad \dots (22)$$

$$+ F_0 \theta_0' + (1 + 2\eta\gamma) Nb \theta_0' H_0'$$

$$+ (1 + 2\eta\gamma) Nb G_0' \phi_0'$$

$$+ 2(1 + 2\eta\gamma) Nt \theta_0' G_0' + \varpi G_0 = 0,$$

$$\begin{aligned}
 &(1+2\eta\gamma)H_0'' + Le f_0 H_0' + Le F\phi_0' \\
 &+ 2\gamma H_0' + (1+2\eta\gamma)\frac{Nt}{Nb}G_0'' \quad \dots (23) \\
 &+ 2\gamma\frac{Nt}{Nb}G_0' + Le\varpi H_0 = 0,
 \end{aligned}$$

with boundary conditions

$$\begin{aligned}
 &F_0(0) = 0, F_0'(0) = \sigma F_0''(0), \\
 &G_0(0) = 0, H_0(0) = 0, \quad \dots (24) \\
 &F_0'(\eta) \rightarrow 0, G_0(\eta) \rightarrow 0, \\
 &H_0(0) \rightarrow 0 \quad \text{as } \eta \rightarrow \infty.
 \end{aligned}$$

It should be mentioned that for particular values γ and ε that involved, the corresponding steady flow solutions $f_0(\eta)$, $\theta_0(\eta)$ and $\phi_0(\eta)$, the stability of the steady flow solution is determined by the smallest eigenvalue ϖ_1 . According to Harris *et al.*⁴⁰, the range of possible Eigen values can be determined by relaxing a boundary condition on $F_0'(\eta)$, $G_0(\eta)$ or $H_0(\eta)$. For the present problem, we relax the condition $F_0'(\eta) \rightarrow 0$ as $\eta \rightarrow \infty$ and for a fixed value of ϖ , we solve the system (21) - (23) along with the new boundary condition $F_0''(0) = 1$.

4 Results and Discussion

The nonlinear ordinary differential Eqs (7)-(9) subject to the boundary conditions (10) were solved numerically using a shooting method. This well-known method is an iterative algorithm which attempts to identify appropriate initial conditions for a related initial value problem (IVP) that provides the

solution to the original boundary value problem (BVP). The dual solutions are obtained for shrinking cylinder by setting different initial guesses for the missing values of the reduced skin friction coefficient $f''(0)$, the reduced local Nusselt number $-\theta'(0)$ and the reduced local Sherwood number $-\phi'(0)$, where all profiles satisfy the boundary conditions (10) asymptotically but with different shapes. These methods have been used by the previous researchers such as Bachok *et al.*⁴⁴, Bakar *et al.*⁴⁵, Najib *et al.*⁴⁶ and Zaimi *et al.*⁴⁷ to solve the boundary layer problems with various cases. The physical significant of different involved parameters, namely curvature parameter γ , Brownian motion parameter Nb , thermophoresis parameter Nt , stretching/shrinking parameter ε , Prandtl number Pr and Lewis number Le on the fluid velocity, temperature and nanoparticle concentration distributions as well as on the skin friction coefficient, the heat and mass transfer rates at the wall are analyzed and presented graphically in Figs 1 to 16. The Prandtl number Pr equal to 1 is chosen because of the fact that both, thermal diffusion and momentum diffusion, changes occur at the same rate. Only results for a Prandtl number of 1, that is, effectively the value for air. The comparison of the present results with the existing numerical results is given in Table 1 to show the validity and it is found to be in excellent agreement.

The variations of the reduced skin friction coefficient $f''(0)$, the reduced local Nusselt number $-\theta'(0)$ and the reduced local Sherwood number $-\phi'(0)$ number with stretching/shrinking parameter ε

Table 1 — The values of reduced skin friction coefficient $f''(0)$ for some values of ε and γ .

ε	Bachok <i>et al.</i> ³⁷	Present results		
	$\gamma = 0$	$\gamma = 0$	$\gamma = 0.2$	$\gamma = 0.4$
2	-1.887307	-1.8873066	-1.9778420	-2.0654420
1	0	0	0	0
0.5	0.713295	0.7132949	0.7629071	0.8100575
0	1.232588	1.2325876	1.3378738	1.4366790
-0.5	1.495670	1.4956697	1.6705694	1.8307523
-1	1.328817	1.3288169	1.6297671	1.8836184
	[0]	[0]	[0]	[0]
-1.15	1.082231	1.0822312	1.4850036	1.7911525
	[0.116702]	[0.1167021]	[-0.0401373]	[-0.1382953]
-1.2	0.932473	0.9324735	1.4106103	1.7423618
	[0.233650]	[0.2336498]	[0.0015211]	[-0.1165670]

[] second solution

for several values of the curvature parameter γ are presented in Figs 2, 3 and 4, respectively, when $Pr = 1$, $Le = 2$, $Nb = 0.1$ and $Nt = 0.1$. The chosen value of curvature parameter γ is $\gamma = 0, 0.2$ and 0.4 , where $\gamma = 0$ corresponds to the flat plate. The dual solutions are found to exist for $\varepsilon > \varepsilon_c$, where ε_c is the critical value of ε for which the solutions exists. Based on our computations, the values of ε_c for $\gamma = 0, 0.2$ and 0.4 are $\varepsilon_c = -1.24657, -1.38090$ and -1.49351 , respectively. Further, the solution is unique when $\varepsilon = \varepsilon_c$ and no solution occurs when $\varepsilon < \varepsilon_c$. From

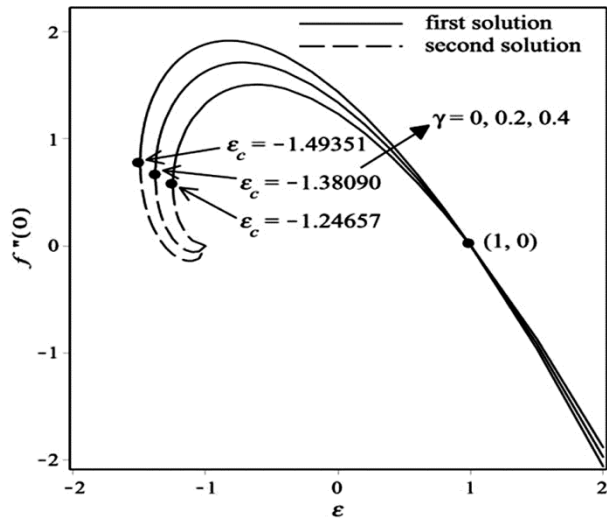


Fig. 2 — Variation of $f''(0)$ with ε for some values of γ when $Pr = 1, Le = 2, Nb = 0.1$ and $Nt = 0.1$.

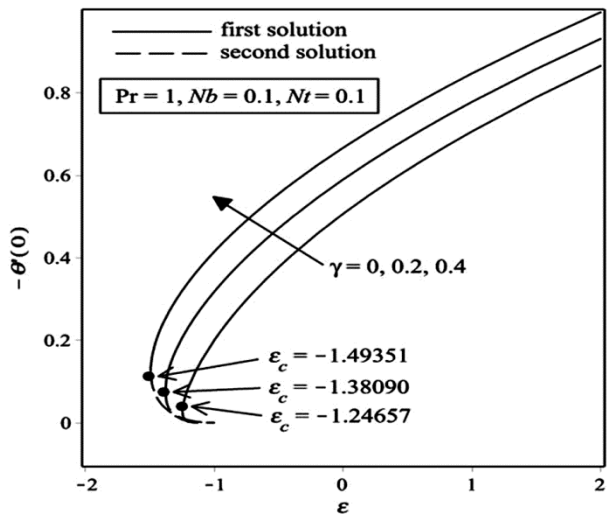


Fig. 3 — Variation of $-\theta'(0)$ with ε for some values of γ when $Pr = 1, Le = 2, Nb = 0.1$ and $Nt = 0.1$.

Fig. 2, it is clearly seen that the value of the reduced skin friction coefficient $f''(0)$ decreases when ε increases, but it has the higher value when γ increases. The opposite trends are found in Figs 3 and 4 where the values of the reduced local Nusselt number $-\theta'(0)$ and the reduced local Sherwood number $-\phi'(0)$ increase as ε increases, however it has the higher value for the greater value of γ . The first solutions in all figures are higher compared to the second solution. The range of ε for which the solution exists is larger for $\gamma > 0$ (cylinder) compared to $\gamma = 0$ (flat plate). This demonstrates that a cylinder increases the range of existence of the similarity solutions to the Eqs (7)-(9) compared to a flat plate. In addition, the boundary layer separation is delayed for a cylinder.

Figures 5 and 6 exhibit the variations of the local Nusselt number $Nu_x Re^{-1/2}$ and the local Sherwood number $Sh_x Re^{-1/2}$ with Brownian motion parameter Nb for several values of the curvature parameter γ , respectively. From Fig. 5, it is observed that the local Nusselt number is a decreasing function of the Brownian motion parameter Nb . As it was mentioned, the increase in Brownian motion parameter Nb tends to decrease temperature gradients in the boundary layer and hence decreases the local Nusselt number. Moreover, it also seen in the figure that the local Nusselt number is a increasing function of the

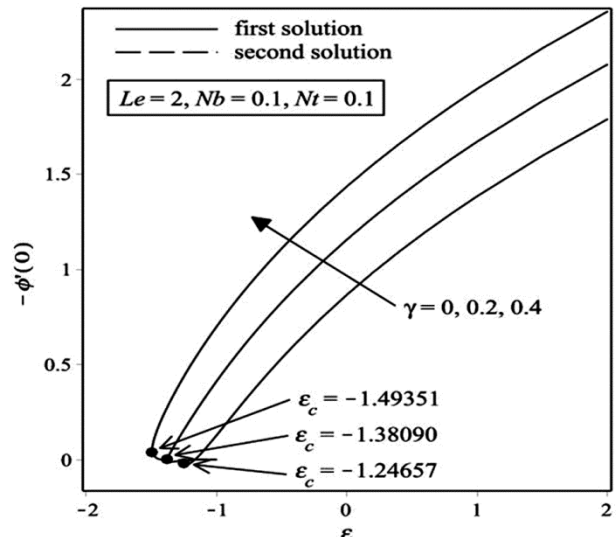


Fig. 4 — Variation of $-\phi'(0)$ with ε for some values of γ when $Pr = 1, Le = 2, Nb = 0.1$ and $Nt = 0.1$.

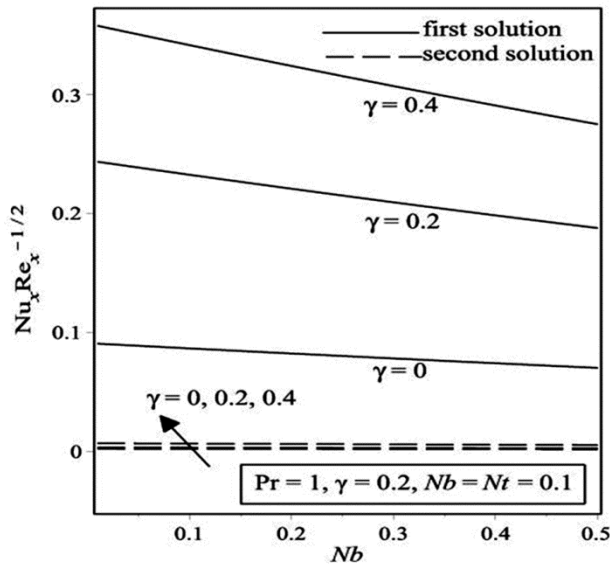


Fig. 5 — Variation of $Nu_x Re_x^{-1/2}$ with Nb for some values of γ when $Pr = 1, Le = 2, \varepsilon = -1.2$ and $Nt = 0.1$.

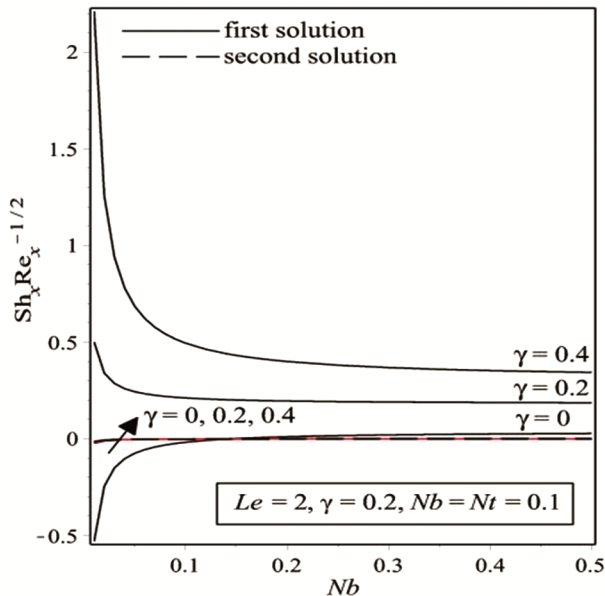


Fig. 6 — Variation of $Sh_x Re_x^{-1/2}$ with Nb for some values of γ when $Pr = 1, Le = 2, \varepsilon = -1.2$ and $Nt = 0.1$.

curvature parameter γ . It is worth mentioning that, the shrinking cylinder is able to increase the heat transfer rate. Next in Fig. 6, the local Sherwood number decreases when Brownian motion parameter Nb increases for cylinder shrinking ($\gamma = 0.2$ and 0.4) but oppositely, when the flat plate is considered, the local Sherwood number is a increasing function of the Brownian motion parameter Nb . However, the values

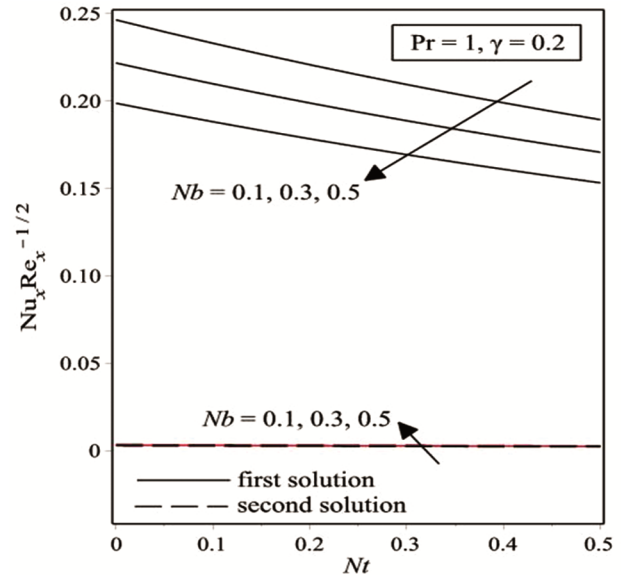


Fig. 7 — Variation of $Nu_x Re_x^{-1/2}$ with Nt for some values of Nb when $Pr = 1, Le = 2, \varepsilon = -1.2$ and $\gamma = 0.2$.

of both the local Nusselt number and local Sherwood number for the first solution is higher compared to the second solution. There were no significant differences in both local Nusselt number and local Sherwood number for the second solution when the value of the curvature parameter γ is increases.

On the other hand, the variations of local Nusselt number with thermophoresis parameter Nt for some values of Brownian motion parameter Nb is depicted in Fig. 7, while the corresponding local Sherwood number is presented in Fig. 8. Figure 7 reveals that there has been a slight decrease in the value of the local Nusselt number when thermophoresis Nt increases. However, when thermophoresis parameter reduces, the local Nusselt number also decreases. The results for local Sherwood number with thermophoresis parameter Nt for several values of Brownian motion parameter Nb in Fig. 8 is similar to that the results obtained in Fig. 7. This phenomenon is may be due to the enhancement of the collisions between particles that results from the increasing of thermophoresis Nt and Brownian motion parameter Nb and hence increase the thermal and nanoparticle concentration boundary layer thicknesses. Thus, reduce the local Nusselt number and local Sherwood number as well as heat and mass flux rates from the surface. The second solution for both the local Nusselt number and local Sherwood number is much lower to the first solution. As shown from these figures, the

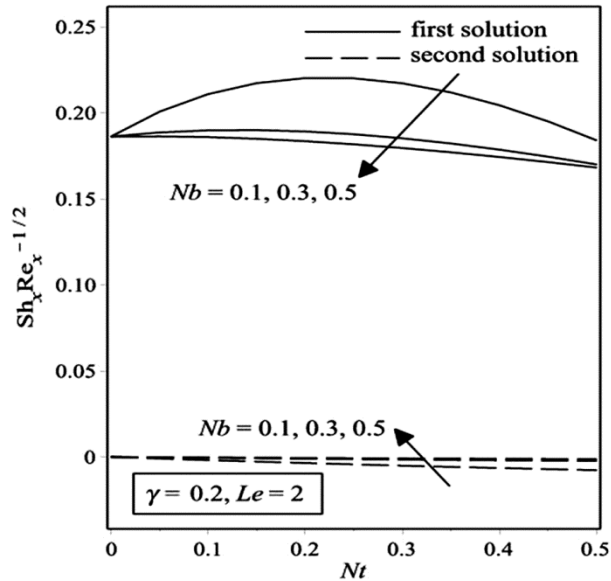


Fig. 8 — Variation of $Sh_x Re_x^{-1/2}$ with Nt for some values of Nb when $Pr = 1, Le = 2, \epsilon = -1.2$ and $\gamma = 0.2$.

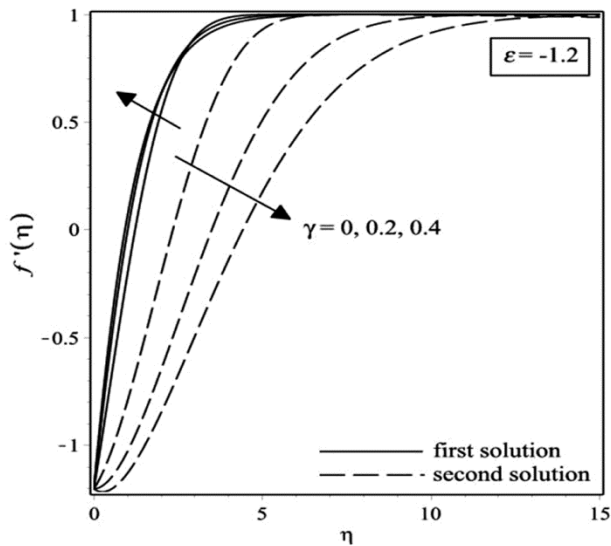


Fig. 9 — Effect of the curvature parameter γ on the velocity profile when $Pr = 1, Le = 2, \epsilon = -1.2, Nb = 0.1$ and $Nt = 0.1$.

local Nusselt number and local Sherwood number for the second solution are not significantly sensitive to the Brownian motion parameter Nb .

Figures 9, 10 and 11 are presented to show the effect of the curvature parameter γ on the velocity, temperature and nanoparticle concentration profiles, respectively, for shrinking cylinder case ($\epsilon = -1.2$). It is seen that there exist two different profiles for a certain value of ϵ , but with different shapes and

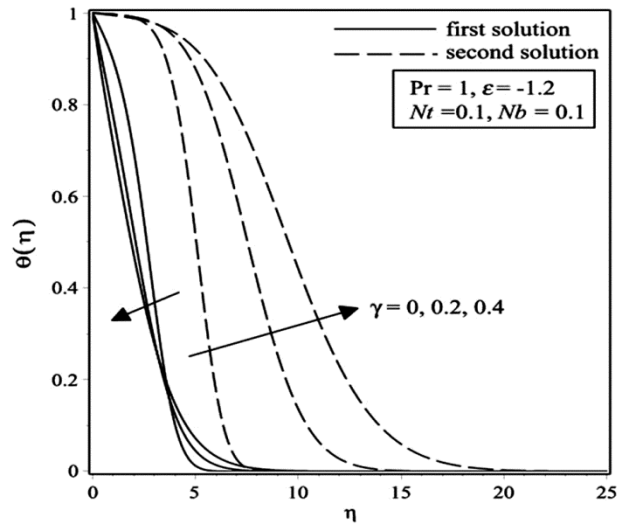


Fig. 10 — Effect of the curvature parameter γ on the temperature profile when $Pr = 1, Le = 2, \epsilon = -1.2, Nb = 0.1$ and $Nt = 0.1$.

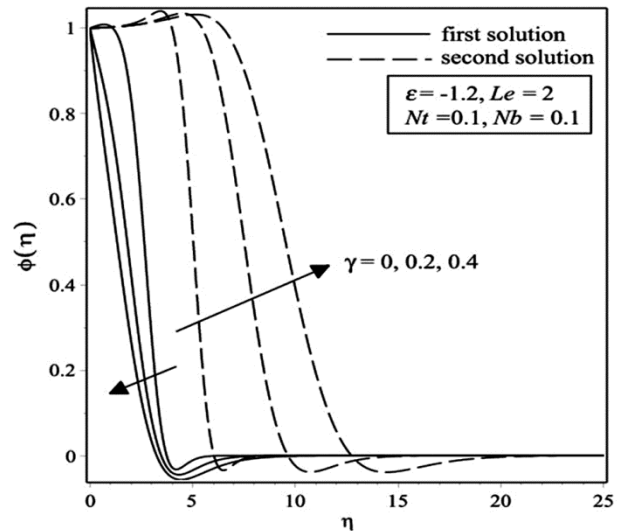


Fig. 11 — Effect of the curvature parameter γ on the nanoparticle concentration profile when $Pr = 1, Le = 2, \epsilon = -1.2, Nb = 0.1$ and $Nt = 0.1$.

boundary layer thickness, which support the existence of dual solutions that illustrated in Figs 2, 3 and 4. In these figures, as curvature parameter γ increases, the velocity, thermal and nanoparticle concentration boundary layer thicknesses for the first solution decreases. In addition, increasing the curvature parameter γ is to decrease the fluid velocity, temperature as well as nanoparticle concentration inside the boundary layer and in consequence increase the velocity, temperature and nanoparticle concentration gradient at the surface of the cylinder.

Hence, it enhances the skin friction coefficient, heat transfer rate and mass transfer rate. Physically, the presents of curvature parameter γ is able to restrict the fluid motion at the surface of the cylinder, heat and mass flux from the surface of cylinder. The opposite trend is found for the second solution where the boundary layer thickness is thicker when curvature parameter γ increases.

The effect of Brownian motion parameter Nb on the temperature and nanoparticle concentration profiles for shrinking cylinder case ($\varepsilon = -1.2$) with other fixed parameters are provided in Figs 12 and 13, respectively. It is apparent from both figures that increasing of Brownian motion parameter Nb may cause the increasing of thermal and nanoparticle concentration boundary layer thicknesses as well as decrease the temperature and nanoparticle concentration gradient in the boundary layer. This phenomenon leads to decrease the local Nusselt number and local Sherwood number. Physically, Brownian motion effect tends to move the nanoparticle from higher concentration to lower concentration and able to warms the fluid in the boundary layer. This motion moves the nanoparticle away from the surface of the shrinking cylinder which are then reduce the thermal and nanoparticle concentration boundary layer thicknesses for both the first and second solution. It is worth mentioning that for the small value of Brownian motion parameter Nb provides important effect on the temperature and nanoparticle concentration.

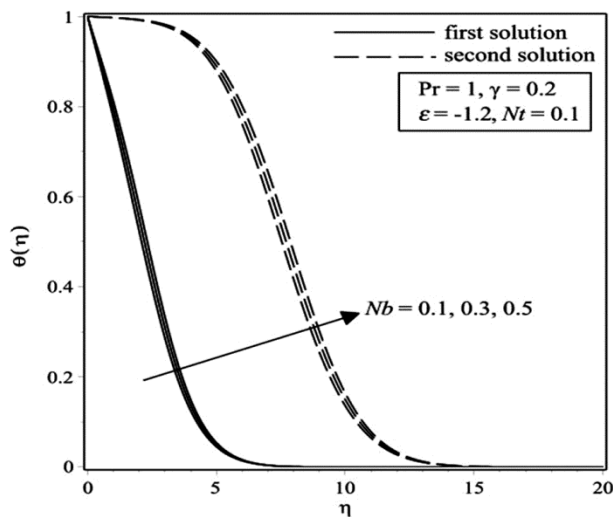


Fig. 12 — Effect of the Brownian motion Nb on the temperature profile when $\gamma = 0.2, Pr = 1, Le = 2, \varepsilon = -1.2$ and $Nt = 0.1$.

Figures 14 and 15 preserve the effect of thermophoresis parameter Nt on the temperature and nanoparticle concentration profiles, respectively, when all parameters are fixed for shrinking cylinder. It is observed in Fig. 14 that the thermal boundary layer thickness increases as thermophoresis parameter Nt increases for both the first and second solution. However, the nanoparticle concentration boundary layer thickness for the first solution in Fig. 15 reduces

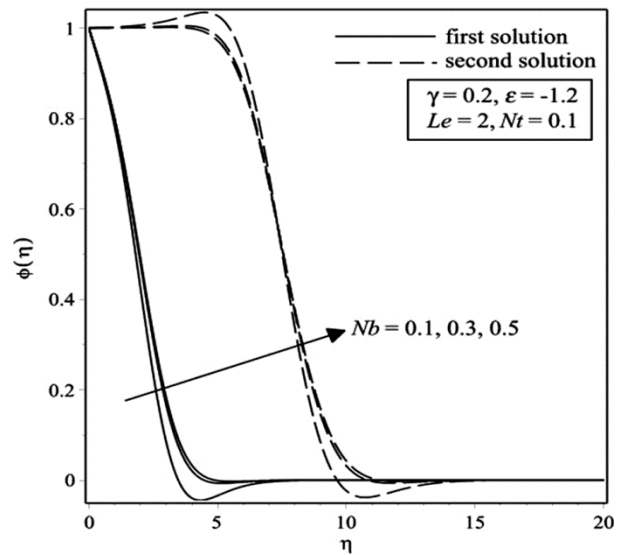


Fig. 13 — Effect of the Brownian motion Nb on the nanoparticle concentration profile when $\gamma = 0.2, Pr = 1, Le = 2, \varepsilon = -1.2$ and $Nt = 0.1$.

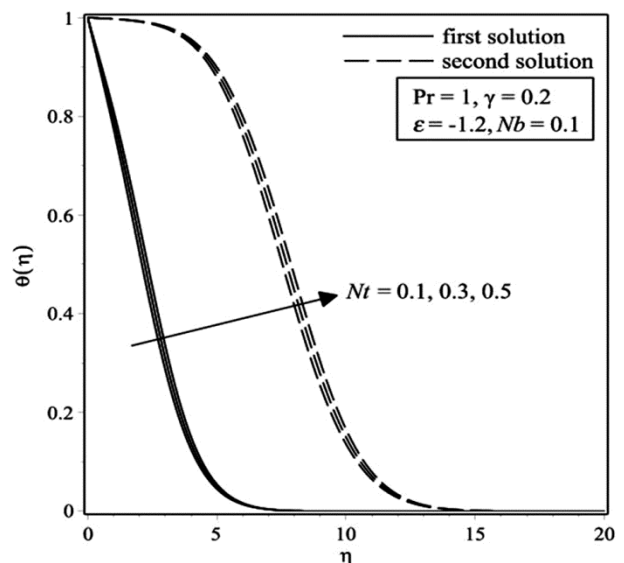


Fig. 14 — Effect of the thermophoresis Nt on the temperature profile when $\gamma = 0.2, Pr = 1, Le = 2, \varepsilon = -1.2$ and $Nb = 0.1$.

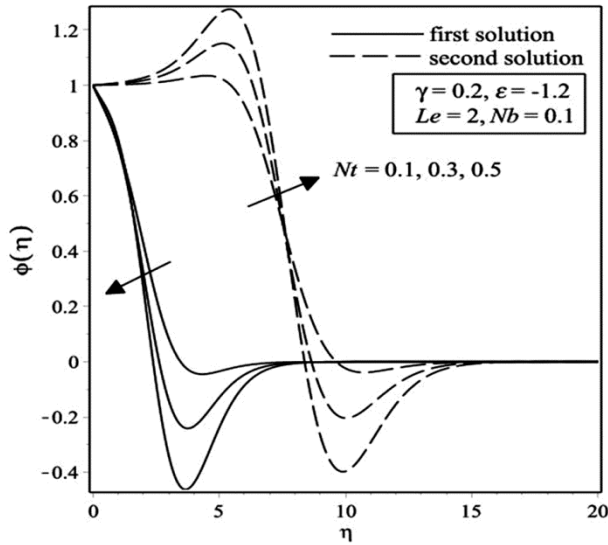


Fig. 15 — Effect of the thermophoresis Nt on the nanoparticle concentration profile when $\gamma = 0.2, Pr = 1, Le = 2, \varepsilon = -1.2$ and $Nb = 0.1$.

when thermophoresis parameter Nt increases, but reversely for the second solution. As we increases the thermophoresis parameter Nt , the temperature gradient decreases and reversely the nanoparticle concentration gradient in the boundary layer increases. Hence, it may lead to decrease the heat transfer rate and increases the mass transfer rate. In nanofluids, thermophoresis effect acts opposite to the temperature gradient and consequently reduces the diffusion of nanoparticles as well as tends to move nanoparticle from hot to cold regions which warm the fluid in the boundary layer.

Further, the temperature profile for some values of Prandtl number Pr for shrinking cylinder is illustrated in Fig. 16. It is found in the figure that the thermal boundary layer thickness increases as Prandtl number Pr increases. Hence, the local Nusselt number decreases. It is worth mentioning that we cannot logically predict sensible change in the thermal boundary layer thickness for $Pr > 5$. The Prandtl number controls the thickness of momentum and thermal boundary layers. When Prandtl number Pr is smaller, the heat diffuses more quickly. Next, the effect of Lewis number Le on the nanoparticle concentration profile is depicted in Fig. 17. It is seen that nanoparticle concentration profile increase as the Lewis number Le increases, which resulting an increasing of the nanoparticle concentration boundary layer thickness and consequently reduces the local Sherwood number. When Lewis number Le is higher,

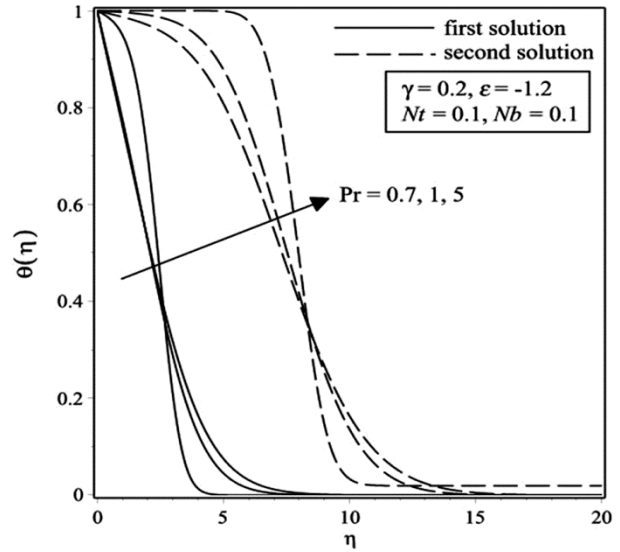


Fig. 16 — Effect of the Prandtl number Pr on the temperature profile when $\gamma = 0.2, Le = 2, \varepsilon = -1.2, Nb = 0.1$ and $Nt = 0.1$.

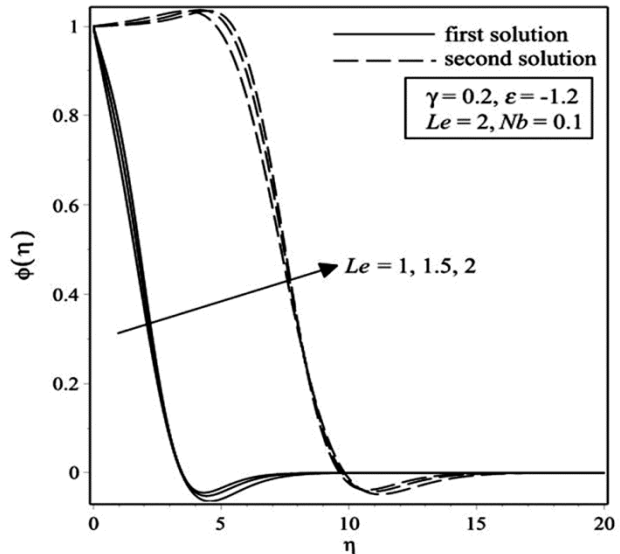


Fig. 17 — Effect of the Lewis number Le on the nanoparticle concentration profile when $\gamma = 0.2, Pr = 1, \varepsilon = -1.2, Nb = 0.1$ and $Nt = 0.1$.

the mass diffusivity is slower, and then increases the nanoparticle concentration boundary layer thickness. As shown from Fig. 17, the nanoparticle concentration profile is not significantly different for the increasing of the Lewis number Le . It is worth mentioning that for all Figs. 9-17 presented into our discussion, the velocity, temperature and nanoparticle concentration profiles are satisfy the far field boundary conditions (10) asymptotically, which support the validity of the numerical results obtained.

Table 2 — Smallest Eigen values ϖ for selected values of γ and ε .

γ	ε	ϖ	
		Upper branch	Lower branch
0	-1.246	0.0622	-0.0614
	-1.24	0.2121	-0.2036
	-1.2	0.3398	-0.3185
0.2	-1.38	0.0314	-0.0306
	-1.35	0.4742	-0.4461
	-1.3	0.7744	-0.6997
0.4	-1.493	0.0601	-0.0597
	-1.49	0.1579	-0.1553
	-1.45	0.2245	-0.2134

The system of linearized problem (21) - (23) along with the new boundary conditions (24) has been applied into `bvp4c` in Matlab software to perform stability analysis. The smallest Eigen value ϖ for some values of ε are displayed in Table 2. It is seen that as the selected value of ε is closer to ε_c , the Eigen value ϖ will approaching zero ($\varpi \rightarrow 0$). As can be seen in Table 2, the value of ϖ is positive (stable solution) for the first solution, while negative value of ϖ (unstable solution) is obtained for the second solution. The solution is stable solution when there only slight disturbance on the flow system that does not affect the flow characteristics, while the unstable solution is stated when there existed initial growth of disturbance that affect the flow system. Thus, the first solution is stable and thus can be realized physically whereas the second solution is not.

5 Conclusions

The two-dimensional stagnation-point flow over a stretching/shrinking cylinder using Buongiorno model is investigated numerically by using shooting method with an application of the Maple software and `bvp4c` codes in Matlab software. The model used incorporates the effects of thermophoresis and Brownian motion. The governing partial differential equations are transformed into ordinary differential equations by means of similarity transformation. The effects of governing parameters such as the curvature parameter, Brownian motion parameter, thermophoresis parameter and stretching/shrinking parameter on the flow, heat and mass transfer characteristics are graphically shown and discussed. Our results show as the curvature parameter increases, the skin friction coefficient, the local Nusselt number and the local Sherwood number increase which represent the heat transfer and mass transfer rates, respectively. Moreover, the increasing of the

Brownian motion parameter and thermophoresis parameter, consequently decreases the heat transfer rate at the cylinder surface. Meanwhile, when the Brownian motion parameter decreases and thermophoresis parameter increases, the mass transfer rate increases. The dual solutions exist for the shrinking cylinder, while a unique solution is obtained for the stretching cylinder. Lastly, the performing of stability analysis shows that the first solution is linearly stable, while the second solution is linearly unstable.

Acknowledgement

The authors gratefully acknowledge the financial support received in the form of a Putra grant scheme (GP-IPS/2016/9512800) from the Universiti Putra Malaysia, Malaysia.

References

- Hiemenz K, *Dingler Polytech J*, 326 (1911) 321.
- Homann F, *Z Angew Math Mech*, 16 (1936) 153.
- Crane L J, *Z Angew Math Phys*, 21 (1970) 645.
- Chiam T C, *J Phys Soc Jpn.*, 63 (1994) 2443.
- Mahapatra T R & Gupta A S, *Acta Mechanica*, 152 (2001) 191.
- Mahapatra T R & Gupta A S, *Heat Mass Transfer*, 38 (2002) 517.
- Ishak A, Nazar R & Pop I, *Meccanica*, 41 (2006) 509.
- Layek G C, Mukhopadhyay S & Samad S A, *Int J Commun Heat Mass Transfer*, 34 (2007) 347.
- Bachok N, Ishak A & Pop I, *Commun Nonlinear Sci Numer Simulat*, 16 (2011) 4296.
- Miklavčič M & Wang C Y, *Quart Appl Math*, 64 (2006) 283.
- Wang C Y, *Int J Nonlin Mech*, 43 (2008) 377.
- Ishak A, Lok Y Y & Pop I, *Chem Eng Commun*, 197 (2010) 1417.
- Lok Y Y, Ishak A & Pop I, *Int J Numer Meth Heat Fluid Flow*, 21 (2011) 61.
- Bhattacharyya K & Layek G C, *Int J Heat Mass Transfer*, 54 (2011) 302.
- Bhattacharyya K & Pop I, *Magnetohydrodynamics*, 47 (2011) 337.
- Bhattacharyya K, Mukhopadhyay S & Layek G C, *Int J Heat Mass Transfer*, 54 (2011) 308.
- Datta P, Anilkumar D, Roy S & Mahanti N C, *Int J Heat Mass Transfer*, 49 (2006) 2366.
- Kumari M & Nath G, *Int J Heat Mass Transfer*, 47 (2004) 969.
- Simal S, Rosselló C, Berna A & Mulet A, *J Food Eng*, 37 (1998) 423.
- Wang C Y, *Phys Fluids*, 31(1988) 466.
- Ishak A, Nazar R & Pop I, *Appl Math Modell*, 32 (2008) 2059.
- Ishak A, Nazar R & Pop I, *Energy Convers Manage*, 49 (2008) 3265.

- 23 Wang C Y & Ng C O, *Int J Nonlin Mech*, 46 (2011) 1191.
- 24 Wang C Y, *Commun Nonlinear Sci Numer Simulat*, 17 (2012) 1098.
- 25 Zaimi W M K A W, Ishak A & Pop I, *J King Saud Univer - Sci*, 25 (2013) 143.
- 26 Lok Y Y & Pop I, *Phys Fluids*, 23 (2011) 083102.
- 27 Mat N A A, Arifin N M, Nazar R & Bachok N, *Appl Math*, 6 (2015) 466.
- 28 Choi S U S, *Proceedings, ASME International Mechanical Engineering Congress and Exposition, San Francisco, Cal, USA, ASME*, 66 (1995) 99.
- 29 Abel M S, Roa P L & Tawade J V, *Int J Mech Eng Tech*, 6 (2015) 87.
- 30 Boungiorno J, *ASME J Heat Transfer*, 128 (2006) 240.
- 31 Rasekh A, Ganji D D & Tavakoli S, *Front Heat Mass Transfer*, 3 (2012) 043003.
- 32 Noghrehabadi A, Ghalebaz M, Izadpanahi E & Pourrajab R, *J Heat Mass Transfer Res*, 1 (2014) 9.
- 33 Tiwari R K & Das M K, *Int J Heat Mass Transfer*, 50 (2007) 2002.
- 34 Gorla R S R, Chamkha A & Al-Meshaie E, *J Naval Architect Marine Eng*, 9 (2012) 1.
- 35 Omar N S, Bachok N & Arifin N M, *Indian J Sci Tech*, 31 (2015) 1.
- 36 Sulochana C & Sandeep N, *Appl Nanoscience*, 6 (2016) 451.
- 37 Bachok N, Ishak A & Pop I, *J Heat Transfer*, 135 (2013) 054501.
- 38 Merkin J H, *J Eng Math*, 20 (1985) 171.
- 39 Weidman P D, Kubitschek D G & Davis A M J, *Int J Eng Sci*, 44 (2016) 730.
- 40 Harris D, Ingham D B & Pop I, *Transport Porous Media*, 77 (2009) 267.
- 41 Najib N, Bachok N, Arifin N M & Ali F M, *Appl Sci*, 8 (2018) 1.
- 42 Bakar S A, Arifin N M, Ali F M, Bachok N, Nazar R & Pop I, *Appl Sci*, 8 (2018) 1.
- 43 Rosca A V & Pop I, *Int J Heat Mass Transfer*, 60 (2013) 355.
- 44 Bachok N, Ishak A & Pop I, *Nanoscale Res Lett*, 6 (2011) 623.
- 45 Bakar N A A, Bachok N & Arifin N M, *Indian J Sci Technol*, 9 (2016) 1.
- 46 Najib N, Bachok N, Arifin N M & Ishak A, *Sci Rep*, 4 (2014) 1.
- 47 Zaimi K, Ishak A & Pop I, *PLoS ONE*, 9 (2014) e111743.